

ON THE 110 keV FEATURE FROM A0535+26: Direct Evidence For A Near-Critical Magnetic Field.

Rafael A. Araya.

Dept. of Physics and Astronomy, The Johns Hopkins University,
Homewood campus, Baltimore, MD 21218.

and

Alice K. Harding.

Laboratory for High Energy Astrophysics,
NASA Goddard Space Flight Center, Greenbelt, MD 20771.

Subject headings: line: formation — magnetic fields — radiative transfer —
stars: neutron — X-rays: stars

Received _____; accepted _____

ABSTRACT

A recent high resolution measurement of an absorption line at $\omega \simeq 110$ keV in the phase-averaged spectrum of A0535+26 (Grove et al. 1994) and the conspicuous absence of a previously reported harmonic feature at $\omega \sim 50$ keV (Kendziorra et al. 1992, 1994) are indicative of cyclotron scattering in a magnetic field of about 10^{13} G. However, controversy has risen over whether a lower field scenario may account for the alleged absence or weakness of a lower energy fundamental harmonic feature. This work explores these two alternatives through the generation of theoretical cyclotron spectra. For lower field models, a cylindrical geometry of the line forming region and the strong angle dependence of the cross section for resonant scattering conspire to fill in a first harmonic at $\omega \simeq 57$ keV. Higher field models ($B \simeq 10.75$ TG), however, yield significantly better fits ($\chi^2_{low}/\chi^2_{high} \sim 71$), thus strengthening the case for a near-critical field ($B_{crit} \simeq 44$ TG). Phase-resolved OSSE spectra are not yet available but would greatly help in resolving this issue.

1. INTRODUCTION

Notwithstanding the lack of spectral evidence for fields above ~ 5 TG, near-critical magnetic fields of neutron stars are invoked to explain some very rapid pulsar spin down rates through magnetic dipole radiation. However, recent spectral observations of the transient X-ray pulsar A0535+26 by the OSSE instrument on board the Compton Gamma Ray Observatory have furnished the most compelling evidence yet for the strongest magnetic field directly observed. Grove et al. (1994) report the detection of a highly significant (F-test $P < 10^{-15}$; Grove, priv. comm.) absorption line feature at $\omega \simeq 110$ keV and the conspicuous absence of an obvious harmonic feature at a lower energy. If due to cyclotron resonant scattering at the fundamental energy, this phase-averaged spectrum would confirm the existence of a magnetic field $B \simeq \frac{1}{4}B_{crit}$ for this object. HEXE observations of an earlier outburst (Kendziorra et al. 1994) showed a feature around 100 keV ($\sim 4.5\sigma$) as well as a weak ($\sim 2\sigma$) feature at $\omega \simeq 50$ keV (the HEXE/TTM instruments on board MIR, have better low energy response but coarser high energy resolution than OSSE).

Cyclotron lines are quasi-harmonic spectral features generated by scattering of resonant photons with the electrons of a magnetized plasma. The interaction is resonant because the electron's momentum eigenvalues perpendicular to \mathbf{B} , $p_\perp/m_e = n$ (B/B_{crit}), are discrete. The resonant photon energies, $\omega_n/m_e = [(1 + 2 n (B/B_{crit}) \sin^2\theta)^{1/2} - 1]/\sin^2\theta$, and the scattering profiles depend on the photon's propagation angle with respect to the field θ . Consequently, the line shapes are heavily influenced by the plasma geometry. As evidenced above, to properly model a source with a near-critical field, $B_{crit} = m^2 c^3/e\hbar$, a relativistic treatment is required regardless of the electron temperature.

Theoretical cyclotron spectra have recently been investigated by Wang, Wasserman and Salpeter (WWS 1988), Wang et al. (1989) and by Alexander and Mészáros (AM 1989). Our scheme improves on previous work by making use of *both* QED magnetic

scattering cross sections and relativistic angle redistribution of photons. In addition, the process of photon spawning (i.e. degrading of photons to lower harmonic energies through electron excitation and subsequent multiple decay) is considered in detail and up to four harmonics are included. For low enough densities and/or high magnetic fields (the requirement for the applicability of our source code), the photon-electron interactions are predominant and collisional terms may be ignored. Specifically, the radiative cyclotron de-excitation rate is given by (Latal 1986) $\nu_r = \alpha m_e [c^2/\hbar] (B/B_{crit})^\beta$ with $\beta \in [2, .5]$ for the undercritical and overcritical field limits respectively. For $B_{12} \simeq 1$, this becomes $\nu_r \sim 2 \times 10^{15} B_{12}^2 \text{ sec}^{-1}$. Comparing the latter expression with that from the collisional rate (Bonazzola, Heyvaerts and Puget 1979), $\nu_c = 5 \times 10^8 (n_e/10^{21} \text{ cm}^{-3}) B_{12}^{-3/2}$, and considering that the continuum optical depths, $\tau_c \stackrel{<}{\sim} 5. \times 10^{-4}$, in the present work give low column densities: $n_l \stackrel{<}{\sim} 7.5 \times 10^{20} \text{ cm}^{-2}$, the neglect of collisions is readily justified. Moreover, the predominance of the magnetized vacuum motivates one chief assumption: the consideration of unpolarized photons only. WWS88 report that averaged (vacuum mode) polarized spectra closely resemble the unpolarized case for optical depths of a few.

A0535+26 is an X-Ray binary transient pulsar with a pulse period of 104 sec. The orbital period is 111 days and the companion of the neutron star is a $12 M_\odot$ Be star. X-Ray episodes for the system are classified into: giant, normal and no burst (Motch et al. 1991). When an outburst does occur, it is typically associated with periastron passage (Hutchings 1984). Both detections of cyclotron line features were made during giant outbursts. Cyclotron line features above 100 keV in the spectra of X-ray pulsars have been difficult to detect for several reasons. First, high resolution detectors with good efficiency at high energies have only recently begun to observe these sources. Second, the intrinsic spectra of many X-ray pulsars turnover at energies above ~ 20 keV. These facts suggest that even if such high fields are common, few may be discovered through their spectral signature. The hardness of the continuum spectrum of A0535+26 below the turnover and its brightness

during outbursts makes it an unusually favorable source for detection of high-energy line features by the OSSE instrument.

Hypothetically, two scenarios for the absence or weakness of a lower energy feature can be envisioned. In the first case, $B \simeq 5$ TG and the geometry of the line forming region combined with the strong angle dependence of the scattering cross section conspire either to fill up a first harmonic at large angles or to form a very shallow and broad fundamental feature at smaller angles. In the other case, the 110 keV absorption line as a fundamental provides direct evidence for a magnetic field $B \simeq 11$ TG. In this *Letter*, we explore these two alternatives by modeling the resonant transfer of unpolarized photons with a Monte Carlo scheme.

2. The February, 1994 event: Giant outburst.

A complete account of the February 1994 event can be found in Grove et al. (1994). The continuum spectrum is modeled as a power law times an exponential: $dN_\omega/(d\omega d\mu) \sim \omega^{-\alpha} \exp(-\omega/kT_c)$. Here α is (minus) the power law index, T_c is the continuum temperature, and $\mu \equiv \cos\theta$ is the cosine of the viewing angle to the field. Their best fit parameters are: $T_c = 17.8$ keV and $\alpha = -.13$. The ‘second harmonic’ (see below) line parameters are: $\omega = 110$ keV, $\tau = 1.8$ (optical depth), and H.W.H.M. = 24 keV. The fits of Grove et al. are consistent with a feature at $\omega \simeq 55$ keV having $\tau \simeq .1$ and H.W.H.M. $\simeq 14.2$ keV. Nevertheless, as pointed out in their paper, the existence of such a lower energy feature is not strictly required for reasonable χ^2 fits to the data. It serves mostly to flatten the spectrum at low energies.

3. A brief description of the code.

Our code makes use of the cyclotron scattering cross section calculated as a 2nd order QED process. The cross section exhibits strong angular dependence and 2nd order effects allow off mass-shell states to contribute to the scattering (Harding and Daugherty 1991; hereafter HD91).

Natural line widths of the cross sections are introduced by using dressed electron propagators and a choice of eigenbasis and spin states which diagonalizes the electron's self-interaction. Thus, cartesian coordinate solutions to the Dirac-Landau equation which are eigenstates of the Sokolov-Ternov spin operator (Herold, Ruder and Wunner 1982) and which diagonalize the mass operator are used. The dressed propagator (i.e. inverse of the D-L equation with a self-energy term) introduces small imaginary (and real) corrections to the resonant energies (Graziani, Harding and Sina 1995). To first order in α , the imaginary part of the correction amounts to the substitution: $\omega \rightarrow \omega - i\frac{\Gamma}{2}$ everywhere in the S matrix. Here Γ is the spin dependent relativistic cyclotron transition rate. Upon squaring of the S matrix element a quasi-Lorentzian line width results (HD91 eq. 20). This prescription is used in our code for the scattering mean-free paths while a Lorentzian line width approximation (absorption approximation, following HD91) allows a semi-analytical inversion of the partial profile convolution integrals to sample the scattering electron momentum P_z .

Furthermore, the code uses a relativistic Maxwellian electron distribution function and includes excitation of Landau levels up to $n = 4$ and their subsequent de-excitation and photon spawning. An approximate relativistic scattering angle redistribution of photons allows for mixing between angle bins.

4. Model Calculation

Two geometries for the scattering region are considered: plane slab (with the magnetic field parallel to the slab normal) and cylindrical (with the field parallel to the cylinder axis). An isotropic continuum photon spectrum is incident from a source at the slab midplane or along the cylinder axis. The escaping photons are accumulated in four ranges of μ (the cosine of the viewing angle to the field). Due to the steepness of the input spectrum, the photons are injected with a flat spectral distribution and are assigned appropriate weight factors. This improves the statistics, but upscattered photons with large weight factors create some noise level in the high energy part of the spectrum. Following Grove et al. (1994), there are two parameters to describe the continuum: α and T_c . Our Monte Carlo code takes three parameters to characterize the line: the electron temperature T_e , the local magnetic field B (assumed uniform), and the minimum value of continuum optical depth τ_c (in the direction parallel to B for a slab and perpendicular to B for a cylinder). A summary of all parameter combination trials is given in Table 1. A representative sample of runs as well as more detail analysis of the trial runs leading to our best fits was presented in Araya and Harding (1996), hereafter AH96-I.

The differences in the line features with various combinations of parameters result from an interplay between the geometry and the variation in the cross section with the photon's angle of propagation with respect to the field. The line profiles are narrower and deeper at large angles, due in part to one dimensional Doppler broadening (cf. HD91). Concurrently, for outgoing photons in a cylindrical scattering region the optical depth at small angles is largest [$\tau_c^{cy}(\theta) = \tau_c/\sin\theta$] while for photons emerging from a slab the optical depth is largest at large angles [$\tau_c^{sl}(\theta) = \tau_c/\cos\theta$] Thus, escaping photons in cylindrical scattering regions tend to redistribute in the line wings from small to large angles, where absorption features may be filled in, while filling in by angle redistribution is much less effective in slab geometries. The (unnormalized) value of τ at the line center may be readily evaluated from the continuum depth: $\tau(\theta) = \tau_c(\theta) * \sigma_{scatt}^{tot}/\sigma_{Thomson}$.

Standard estimates for T_e from the doppler line width, $\Delta\omega_{dop} = \omega_n(2kT_e/mc^2)^{1/2}\cos\theta$, are inadequate for two reasons: first, relativistic kinematics produces broadening even at $\theta = 90^\circ$; second, fundamental features have complex structure resulting from angle mixing and extra injection from spawned photons. Detailed analysis of thermal balance in the line forming region has been addressed by Lamb, Wang and Wasserman (1990), hereafter LWW90, by assuming classical magnetic resonant and non-resonant Compton cross sections. Following the single scattering formalism, assuming line dominated cooling and heating, and assuming isotropic injection, an estimate for the electron temperature yields (eq. 50 of LWW90): $T_e = \omega_{cyc}/(2 + \alpha_{eff})$, with α_{eff} being (minus) the effective power law index at the line. For $\tau \gg 1$, LWW90 produce a numerical estimate from Monte Carlo runs: $T_e \sim \frac{1}{4}\omega_{cyc}$ for $\alpha_{eff} \sim 1$. The latter estimate is not justified for A0535+26 where the continuum at the line(s) has a much larger effective index, $\alpha_{eff} \sim 6.5$ (3.6) at $\omega = 110$ keV (55 keV), and where the optical depth is close to unity. Although we observed that the relativistic and non-relativistic resonant cross sections for $B = 0.24 B_{crit}$ differ by as much as 50% one line width from resonance, the above estimate is used as a guide: $T_e \simeq 12.9$ keV and 9.8 keV for the high and low field models respectively. Nevertheless, in the present work T_e is considered a free parameter determined empirically from the emerging line features. To this end, account is made for the hardness of the incoming continuum as well as the emergent flux distribution in the wings of the fundamental harmonic. Further discussion on the evaluation of T_e is given in AH96-I.

5. Results

5.1. The lower field case

Two foremost restrictions on the emergent theoretical spectra (illustrated in fig 1a and 1c) must be imposed to comply with the data: the first harmonic line must have $E.W. \ll 1$, and the second harmonic feature must be very wide and much more significant ($\tau \sim \text{few}$).

Since the scattering line profile is larger at the first harmonic than at the second, some process must work to fill in the fundamental line feature. Photon spawning and angle redistribution of resonant photons may both enable partial filling of a fundamental feature. Nevertheless, the soft continuum from this source inhibits photon spawning since the number of second harmonic photons is only a small fraction ($\lesssim 1\%$) of the first harmonic photons (the spawned photon contribution is shown in the lower portion fig. 2). On the other hand, angle redistribution from small to large angles does permit filling in of the fundamental absorption feature for cylindrical geometries since the profiles are narrower there (lower portion of fig 1c). In this case, however, overfilling occurs for optical depths compatible with the second harmonic feature, thus producing a sharp *emission* feature at 59 keV as well as a second harmonic line that is too narrow (and very weakly dependent on higher values of T_e).

Alternatively, spectra for $\mu \sim [.5 - .75]$ in both geometries (fig 1a and 1c) exhibit a fairly shallow fundamental feature and a broader second harmonic. For this angle bin, slab geometries display slightly stronger emission wings at the fundamental and a deeper second harmonic with a sharper transition into the high energy continuum compared to their cylindrical counterparts. Nonetheless, the width of the feature at $\omega \sim 110$ keV still fails to match the observation for electron temperatures consistent with spectral hardness, and a significant feature prevails at the fundamental energy. Furthermore, significantly increasing the electron temperature: $T_e \gg 10$ keV (the value implied by eq. 50 of LWW90) enables the first harmonic to become more prominent and fails to considerably broaden the second harmonic. (see AH96-I). Lastly, we note that increasing τ deepens the fundamental, while

decreasing it obliterates the feature at 110 keV.

While our model is able to roughly produce either an ‘undetectable’ first harmonic line or a broad second harmonic, the parameter space for the *mutual* satisfaction of these two conditions is virtually null (we qualify this statement in the conclusions). The best fit lower field model, shown in figure 2, is therefore a compromise between the two constraints mentioned above.

5.2. The higher field case

Figures 1b and 1d illustrate that the closest line feature to that of A0535+26 is provided by a cylindrical geometry in angle bin $\mu > .75$. Our best fit, shown in figure 2 along with the OSSE data, is obtained under these conditions (see caption for details). Note that the value $T_e = 12.94$ obtained from the single scattering estimate of LWW90 is in rough agreement with the fitted value of 12 keV. Moreover, the magnetic field strength $B = 10.75$ TG exceeds the naive estimate based on placing the line centroid at 110 keV: $B \in [9.5, 10.5]$ TG for $\mu \in [0, 1]$.

Several remarks should be made regarding the quality of the fit. The spectrum from the OSSE instrument has very small systematic uncertainties (5% of the flux for $\omega < 80$ keV and 3% for $\omega < 110$ keV (Grove, 1995, priv. comm.)) and our Monte Carlo spectra have statistical noise fluctuations that easily exceed those in the data. The only apparent mismatch for the high field model occurs for the gentler slope of the observed line feature for energies below 110 keV when compared with the theoretical spectrum. One must view this slight discrepancy in light of the limitations of the observation (the data is a phase averaged spectrum) and the limitations of the code (e.g. resulting spectra which are averages over angle bins, representative geometries, etc). We must emphasize that our best

fits have been made using the published flux readings from the OSSE instrument as ‘rigid’ data points, and *not* through the more formal, forward-folding deconvolution of the model with the instrument response function (A scheme for less computationally exhaustive fitting of observational data is not yet available). Therefore, both estimates for the goodness of fit are to be taken not as absolute formal numbers but rather as relative values. The value of the reduced χ^2 is 8.1 for the best high field model and 573 for our best low field spectrum (both shown in fig 2).

6. Conclusions

The present work indicates a very small likelihood that a lower field model would acceptably fit the spectrum of A0535+26. The observational evidence does not seem to support the weak, albeit seemingly detectable, fundamental line that would result at energies of ~ 58 keV. However, the OSSE instrument’s low energy threshold of 45 keV hampers a definite assessment of a line ‘non-detection’. The TTM/HEXE instruments may be better equipped for this lower energy measurement. Exactly what is meant by an ‘un-detectable’ line feature by a particular X-ray instrument is not a trivial question. Work in progress using the HEXE phase *resolved* data has shown the possibility that a fundamental feature with *emission wings* may be completely concealed by the instrument’s response function (Kretschmar et al. 1996).

Note that the uncertainty introduced by using the phase averaged spectrum is determined by the relative dominance of the highest flux phase, if the line is deep enough. Even though no phase resolved spectra are available from OSSE, work in progress with the HEXE data indicates excellent agreement of a formal fit ($\chi^2_{red} = 1.9$) with an essentially identical high field model for the highest flux phase (d) of Kendziorra et al. (1994) (P.

Kretschmar, priv. comm.). This motivates the use of the phase averaged spectrum from OSSE.

Lastly, since the model’s spectral signatures have strong dependencies on geometry and on viewing angle with respect to the field, we cannot rule out that a very radical geometry or an anisotropic incident photon distribution, which we plan to study, may fill up the first harmonic better than can be seen from our representative geometries and isotropic injection models.

In this *Letter* we provide a reasonable appraisal for the various physical parameters and conclude that the 110 keV feature from A0535+26 indeed may come from the highest magnetic field known by *direct* evidence. Further work on phase resolved data is in progress.

Acknowledgments: We would like to thank Ramin Sina for supplying the code to calculate the scattering cross section using Sokolov-Ternov eigenfunctions, P. Kretschmar and J. E. Grove for valuable discussions on the experimental data and A. Szalay for allowing us access to the supercomputer resources at his disposal at the Johns Hopkins University.

T_e (keV)	Magnetic Field strength B (TG), $[B/B_{crit}]$				
	B = 5.25 [.12]	B = 9.5 [.21]	B = 10.36 [.23]	B = 10.75 [.24]	B = 11.14 [.25]
5.	$3.{}^{cy}_{-3}$	$1.{}^{cy,sl}_{-3}$			
10.					$5.{}^{cy,sl}_{-4}$
12	$2.{}^{cy,sl}_{-4}$		$5.{}^{cy,sl}_{-4}$	$5.{}^{cy,sl}_{-4}$	$5.{}^{cy,sl}_{-4}$
12.5	$3.5{}^{cy}_{-4}$				$5.{}^{cy}_{-4}$
14					$8.{}^{cy}_{-4} 1.{}^{sl}_{-3}$
16	$2.5{}^{cy}_{-4}$				
20	$2.{}^{cy,sl}_{-4}$				$2.{}^{cy,sl}_{-4}$
27	$1.{}^{cy}_{-4}$	$1.{}^{sl}_{-3}$			

Table 1: Summary of Parameter Combination Trials. The values of the continuum optical depth τ_c and of the geometry are enclosed. Subscripts are the powers of ten for the value of τ (i.e. $4_{-5} = 4 \times 10^{-5}$.) Cylinder = cy and Slab = sl in the superscripts.

Figure 1: Sample angle-dependent photon count spectra. Each run results from 50000 to 100000 photons injected isotropically. $\mu = \cos\theta$. *Dashed line*: injected continuum. *Solid line*: output scattered spectrum. *Crosses*: single upscattered photons. Points with solid errors are the OSSE phase averaged spectrum. Spectra from slabs are on the top and from cylinders on the bottom. Columns share the values of τ , T_e and B . $T_c = 16.8$ keV and $\alpha = 0$ for a and c (lower field runs). $T_c = 14.5$ keV and $\alpha = 0$ for b and d (higher field runs). See text for notation. The flux normalization is arbitrary.

Figure 2: Best fit theoretical spectra for high field (two top graphs) and low field models (two bottom graphs). The OSSE phase-averaged photon count spectrum for A0535+26 is shown as points with solid error bars (absolute flux for top plot on the right scale). The *dashed horizontal bars* are the model spectra binned according to the energy intervals of the OSSE instrument. The *solid lines* are the same modeled spectra but with equally spaced energy bins. The *dashed line* is the continuum input spectrum. The continuum parameters are: $T_c = 19$. and $\alpha = 0.66$. For $B = 10.75$ TG the line parameters are: angle bin $\mu > .75$, $\tau_c = 5 \times 10^{-4}$ ($\tau \simeq 3.15$) and $T_e = 12$ keV. For $B = 5.25$ TG the line parameters are: angle bin $.75 > \mu > .5$, $\tau_c = 2 \times 10^{-4}$ ($\tau \simeq 1.26$) and $T_e = 12$ keV.

REFERENCES

Alexander, S.G., Mészáros, P. 1989, *Ap.J.*, 344, L1.

Araya, R.A., Harding A.K., *A&A Supp*, Submitted.

Bonazzola, S., Heyvaerts J. and Puget J., 1979. *Astron. Astrophys.*, 78, 53.

Graziani, C., Harding, A.K., Sina, R. 1995, *Phys.Rev.D*, 51, 7097.

Grove, J.E., Strickman, M.S., Johnson, W.N., Kurfess, J.D., Kinzer, R.L., Starr, C.H., Jung, G.V., Kendziorra, E., Kretschmar, P., Maisack, M., Staubert, R. 1994, *Ap.J.*, 438, L25.

Harding, A.K., Daugherty, J.K. 1991, *Ap.J.*, 374, 687.

Herold, H., Ruder, H., Wunner, G. 1982, *Astron. Astrophys.*, 115, 90.

Hutchings, J.B., 1984, *PASP*, 96, 312.

Kendziorra, E., et al. 1992, in Proc. 28th Yamada Conf., *Frontiers of X-Ray Astronomy*, ed. Y. Tanaka and K. Koyama (Tokyo: Univ.Acad.), 51.

Kendziorra, E. et al. 1994, *A&A*, 291, L31.

Lamb, D.Q., Wang, J.C.L., Wasserman, I.M. 1990, *Ap.J.*, 363, 670.

Motch, C., Stella, L., Janot-Pacheco, E., Mouchet, M. 1991, *Ap.J.*, 369, 490.

Wang, J.C.L., Wasserman, I.M., Salpeter, E.E. 1988, *Ap.J.S.*, 68, 735.

Wang, J.C.L., et al. 1989, *Phys. Rev. Lett.*, 63, 1550.

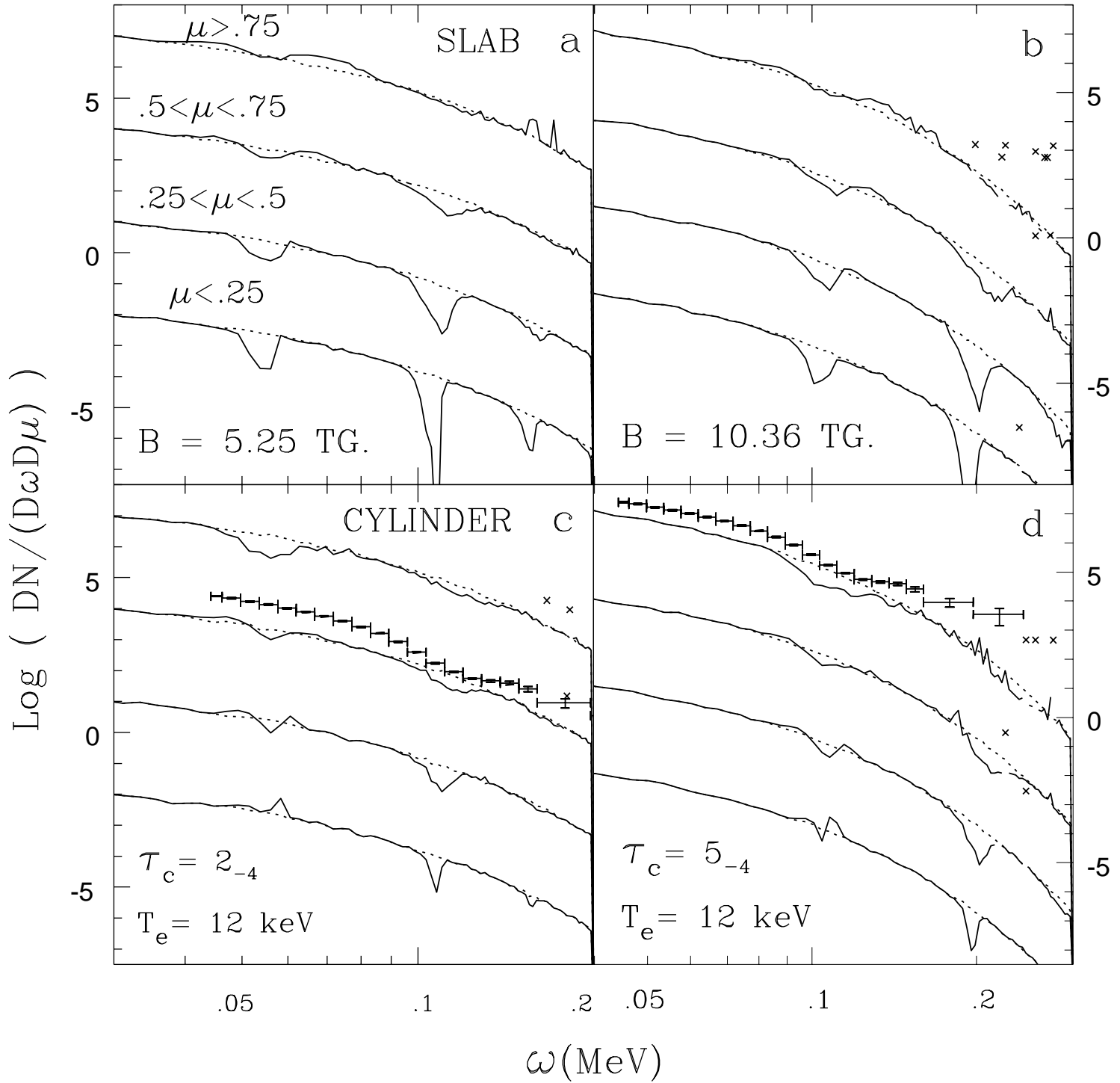


Fig. 1.—

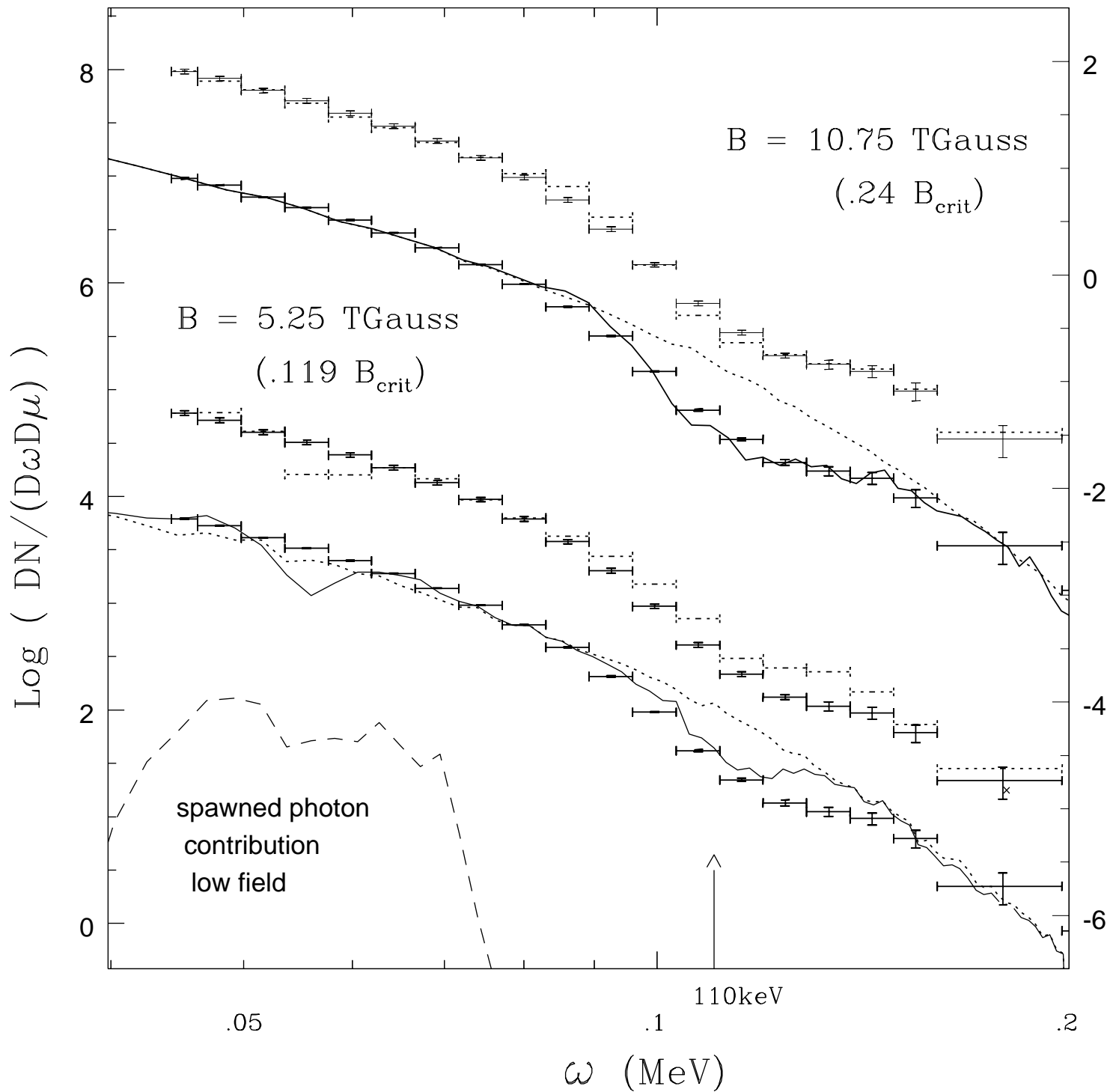


Fig. 2.—